IEEE Access
Multidisciplinary | Rapid Review | Open Access Journal

Received December 8, 2021, accepted January 9, 2022, date of publication January 21, 2022, date of current version February 2, 2022.

Digital Object Identifier 10.1109/ACCESS.2022.3145402

Capture Region of Tactical Missile Equipped With Semi-Active Laser Seeker Using Tobit Kalman Filter

YOUNGJUN LEE[1], SANGMIN LEE[1], YOUDAN KIM[1,2], (Senior Member, IEEE), YONGSU HAN[3], JANGSEONG PARK[3], AND GYEONG-HUN KIM[3]

[1]Department of Aerospace Engineering, Seoul National University, Seoul 08826, Republic of Korea
[2]Institute of Advanced Aerospace Technology, Seoul National University, Seoul 08826, Republic of Korea
[3]LIG Nex1 Company Ltd., Seongnam 13488, Republic of Korea

Corresponding author: Youdan Kim (ydkim@snu.ac.kr)

This work was supported by grants from LIG Nex1 Company Ltd.

ABSTRACT A Tobit Kalman filter-based guidance system was proposed for expanding the capture region of missiles with a strapdown semiactive laser seeker. The characteristics of the semiactive laser seeker were analyzed, and the narrow field-of-view laser seeker model was used based on the analysis. A guidance filter was designed to utilize the saturated region of the seeker to overcome limited maneuverability arising from the narrow field-of-view range. A Tobit Kalman filter is adopted, and the prediction stage was modified so that the Tobit Kalman filter can be applied for nonlinear process models. The filter model for estimating the look angle, LOS angle, and LOS rate was formulated. The proposed guidance filter can estimate the state more robustly even if saturated measurements are given. This study showed that widening the available field-of-view range can lead to the expansion of the capture region. The impact angle control composite guidance and impact angle control guidance with bearing-only measurement were used for intercepting the target with the desired impact angle. Numerical simulations were performed to demonstrate the effectiveness of the proposed method in the saturated region of the seeker and show that the proposed method can expand the size of the capture region.

INDEX TERMS Capture region, impact angle control guidance, semi-active laser seeker, Tobit Kalman filter.

I. INTRODUCTION

Recently, various missile guidance laws have been studied to achieve advanced operational requirements, such as impact angle and impact time, while successfully intercepting targets. In particular, impact angle control, one of the areas of interest, has been actively studied based on various theories, such as optimal impact angle guidance [1]–[5], proportional navigation (PN)-based guidance [6]–[8], and nonlinear control theory-based guidance law [9]–[12].

Additionally, there is an increasing demand for achieving the mission requirements with low-cost missiles. A strapdown seeker may be used as part of the guidance system in low-cost missiles because the strapdown seeker can detect the target accurately although it has a relatively simple mechanical structure [13], [14]. However, one of the significant drawbacks of a strapdown seeker is that the seeker's field of view (FOV) is narrower than a gimbaled seeker [15]. In general, a highly curved trajectory is generated for the missile in engagements with the terminal impact angle constraint, and the target can easily move out of the seeker's FOV [6]. The narrow FOV restricts the maneuverability of the missile because the target must always lie within the seeker's FOV during the engagement for the successful guidance of the missile. Consequently, the narrow FOV significantly reduces the size of the region where the missile can be launched.

Various studies have found the set of initial positions from which missiles can effectively strike a given target. The capture region of a guidance law refers to the set of available initial conditions on which the missile can intercept the target by following the guidance law. Many researchers have analytically derived the capture regions of specific guidance laws [16]–[21]. The launch acceptability region (LAR) denotes the area in a space representing initial launchable

The associate editor coordinating the review of this manuscript and approving it for publication was Ãngel F. García-Fernández.

positions of guided weapons with a high probability of interception, which is a closer concept to a practically used decision-making tool, not for analysis [22]. Studies have also been conducted to estimate the LAR accurately [23]–[25].

A semiactive laser (SAL) seeker was considered the seeker of the missile in this study. Due to the operation method of the SAL seeker's 4-quadrant laser receiver, there is an area in which only saturated measurement information can be obtained over the seeker's FOV [26]. These areas are called saturated regions. That is, the measurement value of the seeker was given as a saturated value in this region, and therefore loss occurs in the target information. A proper filter design was necessary to consider the measurement in the saturated region.

Research has been conducted on guidance filters that estimate the line-of-sight rate with strapdown seekers [27]–[30]. Studies such as [28]–[30] are based on the Kalman filter (KF) but focused on the case in which the target remains in the region where the measurement is not saturated. Filters based on the standard KF do not operate well when saturated measurements are given. However, a guidance filter can still operate even when the measurement slightly goes out of the unsaturated region and returns inside that region after a while.

A Tobit Kalman filter (TKF) is a filter of the standard KF that fits the specialized purpose [31], [32]. The update stage of the TKF is formulated based on a measurement model with saturation, unlike the standard KF. Consequently, the TKF can estimate the state well under proper conditions even if the saturated measurement is given. Theoretical studies based on the TKF have been conducted to cope with various problems that may arise in real situations, such as fading measurement [33] or colored signals [34].

Note that saturated measurement can be thought of as a particular case of nonlinear measurement. Several nonlinear filters, such as an unscented Kalman filter (UKF) [35] or particle filter (PF), can be applied to address the saturation in measurement. However, these filters generally have heavy computational loads. However, the TKF was shown to have significant advantages in computational time, whereas there is no degradation in performance compared to UKF or PF [32]. Therefore, the TKF is one of the reasonable choices for the guidance filter that has to be run in real-time while considering the saturation of the measurement.

In this study, the impact-angle-controlled interception of missiles with limited performance equipment is considered. For this problem, guiding a missile to admissible initial launch positions could be one of the challenging issues in practice because the capture region might be significantly small. Therefore, making more initial conditions available, that is, expanding the capture region, could be one of the alternatives to relieve this issue. Although there have been numerous studies on obtaining the capture region [16]–[21], few studies have been reported about expanding the capture region. In this aspect, one of the main contributions of this study is improving the possibility of mission success by expanding the capture region with the proposed guidance filter.

A planar engagement with a terminal impact angle constraint was considered. The SAL seeker was simply modeled as a measurement model with additive Gaussian noise and subsequent saturation. A guidance filter was designed based on the TKF. The process model of the filter was derived using the relative kinematics. The basic formulation of the TKF was modified to incorporate the nonlinear process model.

The designed guidance filter was combined with an impact angle control guidance law to form a guidance system. Two different guidance laws that can consider the FOV limit of the missile were chosen, which were impact angle control composite guidance (IACCG) laws [6] and impact angle control guidance with bearing-only measurements (IACGBOM) [36]. One advantage of both guidance laws is that they require only the information that can be estimated from the seeker measurement. Only bearing measurements such as the LOS angle and look angle are required for IACGBOM. In the case of IACCG, an LOS rate is also required in addition to the LOS angle and look angle.

The contributions of this study can be summarized as follows. First, the method to expand the capture region of a tactical missile in engagement with the terminal impact angle constraint was proposed by designing a guidance filter that can utilize the characteristics of the SAL seeker based on the TKF. Second, the basic formulation for the TKF in [31], [32] was modified to incorporate a nonlinear process model, and the modification was validated through numerical simulations.

This study is organized as follows. In Section II, the preliminaries on the Tobit Kalman filter and analysis on the characteristics of the SAL seeker are presented. In Section III, the problem statement is explicitly described, including the planar engagement geometry, the overall structure of the homing loop, the SAL seeker model, and the definition of the capture region. In Section IV, the proposed guidance filter and adopted guidance laws are explained. In Section V, numerical simulations are performed to demonstrate the effectiveness of the proposed method. The proposed TKF-based guidance filter was compared with an extended Kalman filter (EKF)-based guidance filter. Additionally, the capture region of the guidance system was compared for the proposed method and the EKF-based method. Finally, Section VI concludes this study.

II. BACKGROUND

A. TOBIT KALMAN FILTER

In this section, the mathematical formulation of the TKF is explained. The standard KF cannot be applied to a model where the measurement may be saturated because the KF assumes that the distribution of the measurement is Gaussian. However, the TKF, a modified KF method, can be applied to a model considering measurement saturation.

The basic formulation and results of the TKF are reviewed first [32]. Then, modification for incorporating a nonlinear process model is introduced.

1) BASIC FORMULATION

Consider the following process and measurement model.

$$x_k = Fx_{k-1} + w_{k-1} \tag{1}$$

$$z_k^* = Hx_k + v_k \tag{2}$$

$$z_k = \begin{cases} z_k^*, & \tau_l < z_k^* < \tau_h \\ \tau_l, & z_k^* \le \tau_l \\ \tau_h, & z_k^* \ge \tau_h \end{cases} \tag{3}$$

where k denotes the time step, $x_k \in \mathbb{R}^{n\times 1}$ is the state vector, $z_k \in \mathbb{R}^{m\times 1}$ is the measurement vector, $F \in \mathbb{R}^{n\times n}$ is the state transition matrix, and $H \in \mathbb{R}^{m\times n}$ is the measurement matrix. $\tau_h \in \mathbb{R}^{m\times 1}$ is the vector of upper threshold values for saturation, and $\tau_l \in \mathbb{R}^{m\times 1}$ is the vector of lower threshold values for saturation. The intermediate variable z_k^* is called the latent variable. The process noise w_k and measurement noise v_k follow the zero-mean white Gaussian with covariance matrices $Q \in \mathbb{R}^{n\times n}$ and $R \in \mathbb{R}^{m\times m}$, respectively. The covariance matrix R for the measurement noise is assumed to be a diagonal matrix having the following form:

$$R = \text{diag}\left(\sigma(1)^2, \sigma(2)^2, \cdots, \sigma(m)^2\right) \tag{4}$$

meaning that the measurement noise is independent across measurements.

The difference between the TKF and the standard KF lies in the measurement model. In the TKF, the measurement is obtained by saturating the latent variable, which results in a different measurement distribution from that of the KF. The conditional distribution of the measurement z_k given x_k is a *truncated* Gaussian distribution for the TKF, while it is an ordinary Gaussian distribution for the KF. The mean and covariance of the measurement also change from those of the KF.

The update stage of the state estimation should be modified accordingly. The state estimate is corrected using the current measurement in the update stage. The update equation to obtain the current estimate may be written as

$$\hat{x}_k = \hat{x}_k^- + K_k\left(z_k - E\left[z_k\right]\right) \tag{5}$$

where $\hat{x}_k^-$ denotes the prior estimate, $\hat{x}_k$ denotes the posterior estimate, and K_k denotes the Kalman gain. The optimal value for K_k is determined by minimizing the posterior state error covariance. A diagonal matrix $v_k \in \mathbb{R}^{m\times m}$ is introduced to concisely express the optimal Kalman gain. Each i th diagonal element $v_k(i,i)$ $(1 \le i \le m)$ is defined as a random variable that follows the Bernoulli distribution given as:

$$v_k(i,i) = \begin{cases} 1, & \tau_l(i) < z_k^*(i) < \tau_h(i) \\ 0, & \text{otherwise} \end{cases} \tag{6}$$

where $\tau_l(i)$, $\tau_h(i)$, and $z_k^*(i)$ denote the i th element of τ_l, τ_h, and z_k^*, respectively. That is, $v_k(i,i)$ has a value of 1 only when the i th element of the measurement z_k is not saturated. The expectation of v_k is given as:

$$E\left[v_k\right] = \text{diag}\left(\Phi\left(\frac{\tau_h(i) - (Hx_k)(i)}{\sigma(i)}\right) - \Phi\left(\frac{\tau_l(i) - (Hx_k)(i)}{\sigma(i)}\right)\right) \tag{7}$$

where Φ denotes the cumulative distribution function for the standard Gaussian. Additionally, the variance of v_k conditioned on the measurements not being saturated can be expressed as

$$E\left[v_k v_k \left(v_k v_k\right)^T\right] = \text{diag}\left(\text{Var}\left(v_k(i) | \tau_l(i) < z_k(i) < \tau_h(i)\right)\right) \tag{8}$$

Refer to the Appendix for more detailed expressions. The optimal Kalman gain K_k and posterior state error covariance P_k can be obtained as

$$K_k = P_k^- H^T E\left[v_k\right] \left(E[v_k^T] H P_k^- H^T E[v_k] + E\left[v_k v_k (v_k v_k)^T\right]\right)^{-1} \tag{9}$$

$$P_k = \left(I_{n\times n} - K_k E\left[v_k^T\right] H\right) P_k^- \tag{10}$$

where P_k^- is the prior state error covariance. Now, let us define $\tilde{H}_k$ and $\tilde{R}_k$ as

$$\tilde{H}_k = E\left[v_k^T\right] H \tag{11}$$

$$\tilde{R}_k = E\left[v_k v_k \left(v_k v_k\right)^T\right] \tag{12}$$

The above expressions can be simplified as

$$K_k = P_k^- \tilde{H}_k^T \left(\tilde{H}_k P_k^- \tilde{H}_k^T + \tilde{R}_k\right)^{-1} \tag{13}$$

$$P_k = \left(I_{n\times n} - K_k \tilde{H}_k\right) P_k^- \tag{14}$$

Note that the above expressions can be thought of as the same expression in the KF except that the measurement matrix H and measurement noise covariance matrix R are replaced with the modified matrix $\tilde{H}_k$ and $\tilde{R}_k$, respectively.

The prediction of the state estimate was performed in exactly the same way as the KF. The prior state estimate $\hat{x}_k^-$ and prior state error covariance P_k^- at the current time instant are predicted using the previous state estimate $\hat{x}_{k-1}$ and state error covariance P_{k-1} as

$$\hat{x}_k^- = F\hat{x}_{k-1} \tag{15}$$

$$P_k^- = FP_{k-1}F^T + Q_{k-1} \tag{16}$$

In (7), (8), knowledge of the actual state value x_k is required to evaluate the expressions used for the update stage. The following assumption allows replacing the actual state value x_k with the estimated state value $\hat{x}_k^-$ instead.

Assumption 1: State prediction was assumed to provide a reasonably accurate estimate of the state with small estimation errors.

In other words, the prior estimate obtained from the prediction stage had to be accurate enough for the update stage

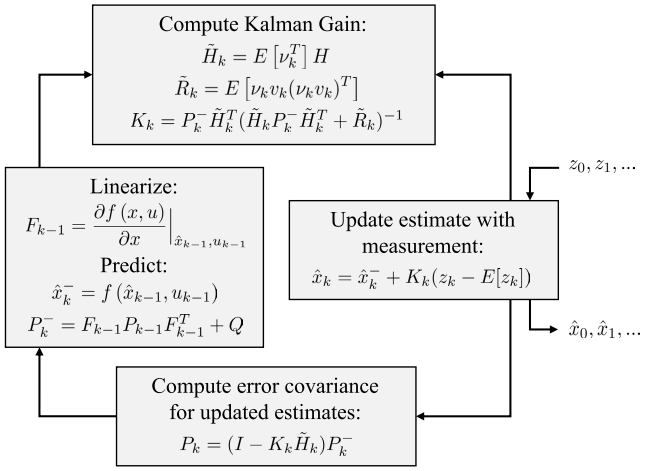

FIGURE 1. The prediction and update stages for the TKF.

to perform as expected. The entire filter's performance may degrade if the prior estimate contains a large estimation error.

2) MODIFICATION FOR A NONLINEAR PROCESS MODEL

The guidance filter considered in this study contained a nonlinear model as the process model. The filter algorithm described in the previous subsection was modified to incorporate a nonlinear process model using linearization as in the EKF. Consider the following nonlinear process model

$$x_k = f(x_{k-1}, u_{k-1}) + w_{k-1} \tag{17}$$

where $u_k \in \mathbb{R}^{l\times 1}$ is the control vector and function $f(\cdot)$ can be nonlinear. The predicted state estimate $\hat{x}_k^-$ and state error covariance P_k^- are given as

$$\hat{x}_k^- = f\left(\hat{x}_{k-1}, u_{k-1}\right) \tag{18}$$

$$P_k^- = F_{k-1} P_{k-1} F_{k-1}^T + Q \tag{19}$$

$$F_{k-1} = \frac{\partial f(x,u)}{\partial x}\Big|_{\hat{x}_{k-1}, u_{k-1}} \tag{20}$$

The prediction equations (15) and (16) are simply replaced with (18)-(20).

The prediction and update stages for the TKF with the modification for a nonlinear process model are shown in Fig. 1.

B. ANALYSIS OF THE CHARACTERISTICS OF SAL SEEKER

In this section, the characteristics of the SAL seeker are described. A laser-guided weapon is employed based on the combination of a laser designator and SAL seeker. The laser designator emits a laser signal consisting of pulses with short duration and high power toward the target, which can be located either on an aerial vehicle or the ground. The external designator illuminates the target. The laser signal is reflected on the surface of the target and reaches the SAL seeker mounted on the missile. Once the seeker receives the laser signal, the information necessary for guidance is estimated from the detected signal.

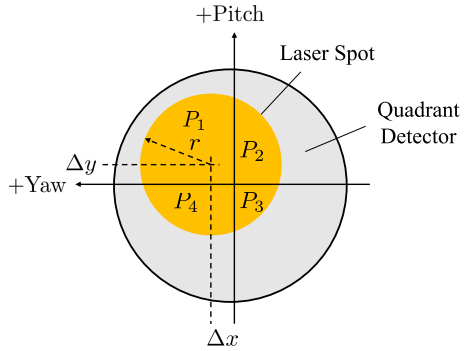

FIGURE 2. SAL seeker plane with 4-quadrant detector.

An SAL seeker with a 4-quadrant detector is widely used in many laser-guided weapons [26]. The SAL seeker considered in this study was also assumed to have a 4-quadrant detector. Fig. 2 shows the seeker plane and the laser spot.

The seeker plane is divided into quadrants, where each quadrant can measure the power of the received laser signal. Information on the target can be obtained based on the fact that the power of the laser signal measured in each quadrant varies according to the laser spot. The measured location of the laser spot Δx, Δy can be approximated in the following form [26].

$$\frac{\Delta y}{r} = \frac{(P_1 + P_2) - (P_3 + P_4)}{P_{total}} \tag{21}$$

$$\frac{\Delta x}{r} = \frac{(P_1 + P_4) - (P_2 + P_3)}{P_{total}} \tag{22}$$

where r is the radius of the laser spot, P_1, P_2, P_3, P_4 are powers received in quadrants 1, 2, 3, and 4, respectively, and $P_{total} = P_1 + P_2 + P_3 + P_4$ is the total power received in the seeker plane. The pitch look angle θ_l and the yaw look angle ψ_l to the target can be approximated as $\theta_l = \frac{\Delta y}{f}$ and $\psi_l = \frac{\Delta x}{f}$, respectively, where f is the focal length of the seeker, assuming that deviations of the laser spot from the center of the seeker plane are small in both the pitch direction and the yaw direction.

The typical relation between the actual and measured look angles is shown in Fig. 3, which was obtained numerically using (21), (22). Fig. 3a) shows the measured θ_l of the laser spot with respect to its actual θ_l and ψ_l. Fig. 3b) shows the measured ψ_l of the laser spot with respect to its actual θ_l and ψ_l. Some important characteristics can be inferred from the figures.

First, the measured θ_l depended almost only on the actual θ_l and did not depend on the actual ψ_l. Likewise, the measured ψ_l depended almost only on the actual ψ_l and did not depend on the actual θ_l. Therefore, the measurements of look angles in the pitch direction and yaw direction can be considered to be independent of each other.

In addition, the results showed that the measurement region was composed of a linear region and saturated regions. The measurement for θ_l between ± 7.5 degrees was almost the same as its actual value (linear region) and was saturated

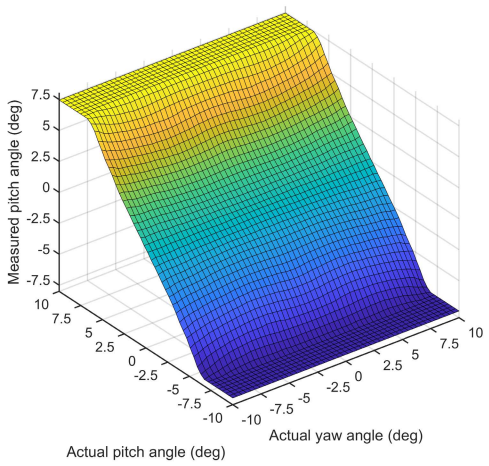

(a) Pitch angle measurement of the SAL seeker

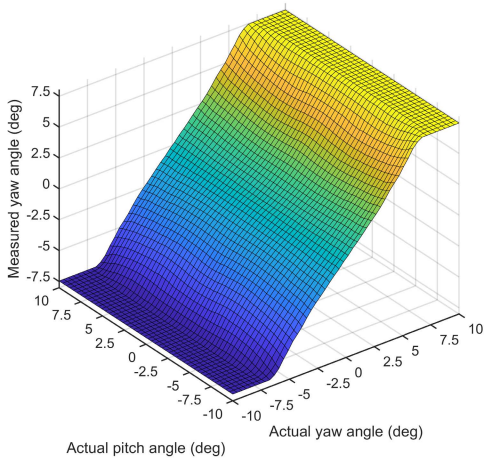

(b) Yaw angle measurement of the SAL seeker

FIGURE 3. Relation between the actual and measured look angles.

above ±7.5 degrees (saturated region). The small discrepancy between the measurement and actual value in the linear region was due to the approximation error in (21). Similar properties were observed for the yaw angle.

III. PROBLEM STATEMENT

This study aimed to propose a guidance system based on the TKF that can expand the capture region of the missile. A planar engagement was considered in this study. The engagement geometry and the equations of the relative kinematics are given in Section III-A. The overall structure of the homing loop is explained in Section III-B. Then, a simple mathematical model for the SAL seeker is given in Section III-C based on the properties of the SAL seeker. Finally, the definition of the capture region is presented in Section III-D.

A. PLANAR ENGAGEMENT GEOMETRY

The engagement geometry between a missile and a target is shown in Fig. 4. The frame $X_I O_I Y_I$ represents the inertial coordinate frame. V_M and γ_M denote the speed and flight

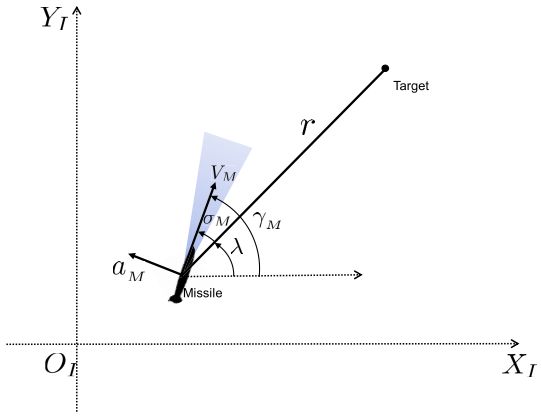

FIGURE 4. Planar engagement geometry.

path angle of the missile, respectively. The missile angle of attack (AOA) was assumed to be negligible. λ and r are the line-of-sight (LOS) angle and the relative distance, respectively. a_M represents the normal acceleration of the missile. σ_M is the look angle defined as the difference between the LOS angle and flight path angle of the missile under the assumption of small AOA.

$$\sigma_M = \gamma_M - \lambda \tag{23}$$

A gradually shaded triangle in the figure describes the FOV range of the missile.

According to the variables defined in Fig. 4, the nonlinear equations describing the relative motion of the missile toward a stationary target can be expressed as

$$\dot{r} = -V_M \cos\sigma_M \tag{24}$$

$$\dot{\lambda} = -\frac{V_M}{r}\sin\sigma_M \tag{25}$$

where the speed V_M of the missile was assumed to be constant in this study. a_M is applied perpendicular to the missile velocity vector. Then, the time derivative of the flight path angle can be written as

$$\dot{\gamma}_M = \frac{a_M}{V_M} \tag{26}$$

B. HOMING LOOP

Fig. 5 shows the overall structure of the homing loop of the missile. The homing loop consists of the guidance filter, guidance law, autopilot, missile dynamics, in which the main interest of this study was the guidance filter and the guidance law indicated as the gray-colored blocks in Fig. 5. Additionally, the missile has an inertial navigation system (INS) and an SAL seeker. In the figure, $\hat{\lambda}$, $\hat{\dot{\lambda}}$, and $\hat{\sigma}_M$ represent the estimated LOS angle, LOS angle rate, and look angle, respectively. θ and q mean the pitch angle and the angular velocity of the missile, respectively. θ can be regarded as the same as γ_M assuming a small AOA.

There are several assumptions in this structure of the homing loop. First, sufficiently accurate information on the

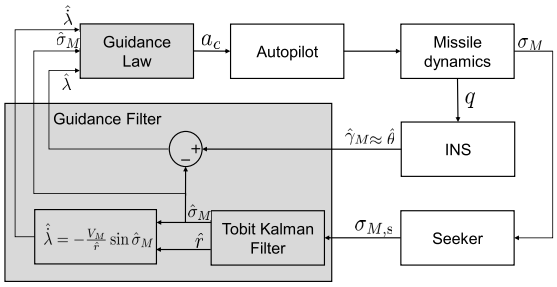

FIGURE 5. The overall structure of homing loop.

missile's attitude was supposed to be given from INS. Then, information on the flight path angle can also be accurately obtained under small AOA assumption. Second, it was assumed that there was no time delay in the seeker so that the parasitic effect can be ignored [37]. Finally, the autopilot is modeled as the first-order lag system with constant time delay.

Note that information on the relative distance between the missile and the target cannot be obtained from any of INS or the seeker. The measurement of the look angle obtained from the seeker was the only information on the relative kinematics. Therefore, the proposed guidance filter may not accurately correct the estimate of the relative distance. The estimate of the relative distance may diverge slowly due to the loss of observability.

C. SAL SEEKER MODEL

Based on the observation given in the Section II-B, it was enough to consider only one of the pitch or yaw angles when a planar engagement scenario was considered. Therefore, the mathematical model of the SAL seeker was simplified as (27), (28).

$$\sigma_M^* = \sigma_M + v \tag{27}$$

$$\sigma_{M,s} = \begin{cases} \sigma_M^*, & \text{for} \quad |\sigma_M^*| < \sigma_{M,\text{sat}} \\ \sigma_{M,\text{sat}}, & \text{for} \quad \sigma_M^* \geq \sigma_{M,\text{sat}} \\ -\sigma_{M,\text{sat}}, & \text{for} \quad \sigma_M^* \leq -\sigma_{M,\text{sat}} \end{cases} \tag{28}$$

where σ_M is the actual look angle, σ_M^* is a latent variable for the look angle, and $\sigma_{M,s}$ is the measured look angle from the seeker. $\sigma_{M,\text{sat}}$ is the saturation threshold of the seeker, and $v \sim N(0, R)$ is the measurement noise following the zero-mean white Gaussian with variance R.

Note that $\sigma_{M,\text{sat}}$ should not be confused with the seeker's FOV limit. $\sigma_{M,\text{sat}}$ is the value dividing the linear region and saturated region where the saturated region is a region *inside* the FOV limit. The saturated region originates from the laser spot reaching only half of the seeker plane, and not from the laser spot getting out of the FOV limit. The FOV limit is denoted as $\sigma_{M,\text{lim}}$.

D. CAPTURE REGION

The capture region was defined as a set of initial conditions on which the missile can be initiated and then results in successful interception by following a specific guidance law. Although the term capture region is usually used for describing the result of a *guidance law*, it is used for the *entire guidance system* in this study. Additionally, the capture region was determined by a numerical method rather than an analytic method because analytically finding the capture region was almost intractable when the entire guidance system was considered.

The initial relative distance r_0 and the initial LOS angle λ_0 were considered components of the initial condition. The continuous space of initial conditions was discretized into a finite set that closely approximates the original space, which was written as Θ_d. Given an initial condition, the conditions of successful interception were set as

$$r_{\text{miss}} \leq \epsilon_r \tag{29}$$

$$|\gamma_M(t_f) - \gamma_d| \leq \epsilon_\gamma \tag{30}$$

$$|\sigma_M(t)| \leq \sigma_{M,\text{lim}} \quad \forall t \in [0,\ t_f] \tag{31}$$

where ϵ_r and ϵ_γ are the maximum acceptable miss distance and terminal impact angle error, respectively. r_{miss} denotes the miss distance, which is the minimum distance between the missile and target. t_f is the time when the missile is at the closest position to the target. $\gamma_M(t_f)$ denotes the actual flight path angle of the missile at t_f, and γ_d denotes the desired terminal flight path angle of the missile. The interception of a single engagement simulation is considered successful if all three conditions were satisfied.

The success rate of the interception $p_N(r_0, \lambda_0)$ for an initial condition (r_0, λ_0) is defined as follows:

$$p_N(r_0, \lambda_0) = \frac{1}{N} \sum_{i=1}^{N} I_i(r_0, \lambda_0) \tag{32}$$

where N is the number of trials, and $I_i(r_0, \lambda_0)$ is an indicator variable that takes 1 when a missile intercepts a target and 0 otherwise in the i th trial ($i = 1, 2, \cdots, N$). $p_N(r_0, \lambda_0)$ can be regarded as a value approximating the probability of successful interception. Then, the capture region C_N is defined as the following discrete set.

$$C_N = \{(r_0, \lambda_0) \in \Theta_d : p_N(r_0, \lambda_0) \geq 0.8\} \tag{33}$$

IV. GUIDANCE SYSTEM

The guidance system of the missie consists of the seeker, guidance filter, and guidance law. In this section, the design for the guidance filter is proposed based on the TKF. Then, guidance laws adopted in this study are explained.

A. THE PROPOSED GUIDANCE FILTER

The process model of the guidance filter was formulated based on the relative kinematics. The measurement model of the guidance filter was formulated based on the seeker model. The look angle σ_M and relative distance r were chosen as the state of the filter. The LOS angle λ and LOS rate $\dot{\lambda}$ were estimated from the estimated state of the filter.

1) PROCESS MODEL

The primary role of the TKF was to estimate σ_M. Therefore, σ_M was chosen as the state. However, not only σ_M but also r was included in the state vector because it was required for estimating $\dot{\lambda}$.

The relationship between σ_M, γ_M, and λ is

$$\sigma_M = \gamma_M - \lambda \tag{34}$$

The look angle rate $\dot{\sigma}_M$ was obtained by differentiating (34) with respect to time as

$$\dot{\sigma}_M = \dot{\gamma}_M - \dot{\lambda} \tag{35}$$

Substituting (25) and (26) into (35), we have

$$\dot{\sigma}_M = \frac{V_M}{r}\sin\sigma_M + \frac{a_M}{V_M} \tag{36}$$

where V_M is constant. According to (36), σ_M and r should be known to get $\dot{\sigma}_M$. However, information on r is not easy to obtain because the missile was assumed not to have any sensor to measure the relative distance directly. The value for r should be estimated using the filter. Therefore, the time derivative of the relative distance was also included in the process model, which is expressed as

$$\dot{r} = -V_M\cos\sigma_M \tag{37}$$

Suppose that the normal acceleration a_M has additive uncertainty which was modeled as white noise with zero mean and variance σ_w^2. Then, the continuous-time process model can be expressed as

$$\begin{bmatrix}\dot{\sigma}_M\\ \dot{r}\end{bmatrix} = \begin{bmatrix}\frac{V_M}{r}\sin\sigma_M\\ -V_M\cos\sigma_M\end{bmatrix} + \begin{bmatrix}\frac{1}{V_M}\\ 0\end{bmatrix}a_M + \begin{bmatrix}\frac{1}{V_M}\\ 0\end{bmatrix}w \tag{38}$$

where w is white noise with zero mean and variance $Q = \sigma_w^2$.

By discretizing (38) using the Euler method, the discrete-time process model is obtained as

$$\begin{bmatrix}\sigma_{M,k+1}\\ r_{k+1}\end{bmatrix} = \begin{bmatrix}\sigma_{M,k}\\ r_k\end{bmatrix} + \begin{bmatrix}\frac{V_M}{r_k}\sin\sigma_{M,k}\\ -V_M\cos\sigma_{M,k}\end{bmatrix}\Delta t + \begin{bmatrix}\frac{\Delta t}{V_M}\\ 0\end{bmatrix}a_{M,k} + w_k \tag{39}$$

where Δt is the discretization time interval, $\sigma_{M,k}$, r_k, and $a_{M,k}$ are the look angle, relative distance, and normal acceleration at time t_k, respectively. w_k is the discrete-time process noise following a zero-mean Gaussian, whose covariance Q_k will be derived below. The above model is expressed as

$$x_{k+1} = f(x_k, u_k) + w_k \tag{40}$$

where $x_k = \left[\sigma_{M,k}\ r_k\right]^T$, $u_k = a_{M,k}$.

To derive the expression for Q_k, the process model (38) is linearized around x_k. Letting $\Delta x = x - x_k$,

$$\Delta\dot{x} = F_k\Delta x + Ga_M + Gw \tag{41}$$

where F_k is a Jacobian matrix consisting of first-order partial derivatives of (38) evaluated at x_k as

$$\begin{aligned} F_k &= \begin{bmatrix}\frac{\partial\dot{x}_1}{\partial x_1} & \frac{\partial\dot{x}_1}{\partial x_2}\\ \frac{\partial\dot{x}_2}{\partial x_1} & \frac{\partial\dot{x}_2}{\partial x_2}\end{bmatrix}_{x=x_k}\\ &= \begin{bmatrix}\frac{V_M}{r_k}\cos\sigma_{M,k} & -\frac{V_M}{r_k^2}\sin\sigma_{M,k}\\ V_M\sin\sigma_{M,k} & 0\end{bmatrix}\end{aligned} \tag{42}$$

and G is defined as

$$G = \begin{bmatrix}\frac{1}{V_M}\\ 0\end{bmatrix} \tag{43}$$

The state transition matrix $\Phi(t) = e^{F_k t}$ of the linearized model (41) can be approximated to the first-order term as

$$\begin{aligned}\Phi(t) &= e^{F_k t}\\ &= I + F_k t + \frac{(F_k t)^2}{2!} + \cdots + \frac{(F_k t)^n}{n!} + \ldots\\ &\approx I + F_k t\end{aligned} \tag{44}$$

The expression for Q_k is obtained from Q and $\Phi(t)$ [38]

$$\begin{aligned} Q_k &= \int_0^{\Delta t}\Phi(\tau)GQG^T\Phi(\tau)^T d\tau\\ &\approx \int_0^{\Delta t}(I + F_k\tau)GQG^T(I + F_k\tau)^T d\tau\\ &= \frac{1}{3}\Delta t^3 F_k GQG^T F_k^T\\ &\quad + \frac{1}{2}\Delta t^2(F_k GQG^T + GQG^T F_k^T) + GQG^T\Delta t\end{aligned} \tag{45}$$

Denoting the (i, j) element of F_k as f_{ij},

$$\begin{aligned} Q_k &= \frac{1}{3}\Delta t^3\frac{\sigma_w^2}{V_M^2}\begin{bmatrix}f_{11}^2 & f_{11}f_{21}\\ f_{11}f_{21} & f_{21}^2\end{bmatrix}\\ &\quad + \frac{1}{2}\Delta t^2\frac{\sigma_w^2}{V_M^2}\begin{bmatrix}2f_{11} & f_{21}\\ f_{21} & 0\end{bmatrix} + \Delta t\frac{\sigma_w^2}{V_M^2}\begin{bmatrix}1 & 0\\ 0 & 0\end{bmatrix}\\ &= \frac{\sigma_w^2\Delta t}{V_M^2}\begin{bmatrix}q_{11} & q_{12}\\ q_{21} & q_{22}\end{bmatrix}\end{aligned} \tag{46}$$

where $q_{11}, q_{12}, q_{21}, q_{22}$ are

$$q_{11} = \frac{1}{3}\Delta t^2 f_{11}^2 + \Delta t f_{11} + 1 \tag{47}$$

$$q_{12} = \frac{1}{3}\Delta t^2 f_{11}f_{21} + \frac{1}{2}\Delta t f_{21} \tag{48}$$

$$q_{21} = q_{12} \tag{49}$$

$$q_{22} = \frac{1}{3}\Delta t^2 f_{21}^2 \tag{50}$$

2) MEASUREMENT MODEL

The look angle measurement is given from the seeker. The measurement model is constructed as follows:

$$z_k^* = \begin{bmatrix}1 & 0\end{bmatrix}\begin{bmatrix}\sigma_{M,k}\\ r_k\end{bmatrix} + v_k \tag{51}$$

$$= Hx_k + v_k \tag{52}$$

$$z_k = \begin{cases} z_k^*, & \text{for} \quad |z_k^*| < \sigma_{M,\text{sat}} \\ \sigma_{M,\text{sat}}, & \text{for} \quad z_k^* \geq \sigma_{M,\text{sat}} \\ -\sigma_{M,\text{sat}}, & \text{for} \quad z_k^* \leq -\sigma_{M,\text{sat}} \end{cases} \tag{53}$$

where z_k^* is a latent variable, v_k is the measurement model additive noise whose mean is zero and the standard deviation is σ_v.

3) ESTIMATION OF THE LOS ANGLE AND RATE

The TKF block in Fig. 5 outputs an estimate of the look angle $\hat{\sigma}_{M,k}$ and the relative distance $\hat{r}_k$ at time step t_k. The LOS angle and rate estimates $\hat{\lambda}_k$, $\hat{\dot{\lambda}}_k$ can be calculated from these outputs.

The estimate of the flight path angle of the missile $\hat{\gamma}_{M,k}$ has approximately the same value as that of the attitude of the missile $\hat{\theta}_k$ under the small AOA assumption. In this study, it was assumed that a sufficiently accurate estimate $\hat{\theta}_k$ is given from INS. Then, the LOS angle estimate $\hat{\lambda}$ is obtained as

$$\hat{\lambda}_k = \hat{\gamma}_{M,k} - \hat{\sigma}_{M,k} \tag{54}$$

where $\hat{\gamma}_{M,k}$ denotes the flight path angle estimate of the missile at time step t_k. The LOS angle rate estimate $\hat{\dot{\lambda}}$ is obtained by using (25) with $\hat{\sigma}_{M,k}$ and $\hat{r}_k$ as follows:

$$\hat{\dot{\lambda}}_k = -\frac{V_M}{\hat{r}_k} \sin \hat{\sigma}_{M,k} \tag{55}$$

B. GUIDANCE LAW

Two different guidance laws IACGBOM [36] and IACCG [6] were adopted. Both guidance laws can impose the terminal impact angle constraint while considering the seeker's FOV limit. The first one, IACGBOM, is a guidance law based on sliding mode, requiring only the look angle and LOS angle information. The other one, IACCG, is a composite guidance law switching between two guidance laws. IACGBOM has the advantage of requiring less information than IACCG. However, its application is limited only to a stationary target, while IACCG can also be applied to a nonmaneuvering moving target.

1) IMPACT ANGLE CONTROL GUIDANCE WITH BEARING-ONLY MEASUREMENTS

In IACGBOM, the guidance command is derived based on the sliding mode technique so that error variables related to the interception condition and impact angle constraint converge to zero. The FOV limit constraint is satisfied by introducing a sigmoid function.

Let us denote the desired terminal flight path angle of the missile as γ_d, which is determined by the prescribed impact angle constraint. Error variables e_1 and e_2 are defined as

$$e_1 = \lambda - \gamma_d \tag{56}$$

$$e_2 = \sigma_M \tag{57}$$

Satisfying both conditions $e_1 = 0$ and $e_2 = 0$ leads to interception at the desired impact angle. A sigmoid function sgmf $(\cdot)$ is defined as

$$\text{sgmf}\,(x) = \frac{x}{\sqrt{x^2 + \phi_1^2}} \quad (\phi_1 > 0) \tag{58}$$

Let us denote the sliding surface variable S as

$$S\,(\sigma_M, \lambda) = e_2 - k_1 \text{sgmf}\,(e_1) \quad \left(0 < k_1 < \sigma_{M,\text{lim}}\right) \tag{59}$$

where k_1, ϕ_1 are the user chosen parameters. Note that the value of k_1 should be chosen to be smaller than $\sigma_{M,\text{lim}}$ to keep the look angle within the seeker's FOV limit for the entire engagement.

The guidance law is given as

$$a_M = -\left(\frac{V_M}{R_f} f_2\,(\sigma_M, \lambda) + k_2\right) V_M \tanh(aS) \tag{60}$$

where R_f is the acceptable maximum miss distance, k_2 is a positive constant related to the convergence rate, and

$$f_2\,(\sigma_M, \lambda) = \left(1 + k_1 \frac{\partial}{\partial e_1} \text{sgmf}\,(e_1)\right) |\sin \sigma_M| \tag{61}$$

$$= \left(1 + k_1 \frac{\phi_1^2}{\left(e_1^2 + \phi_1^2\right)^{3/2}}\right) |\sin \sigma_M| \tag{62}$$

In (60), the hyperbolic tangent function tanh$(\cdot)$ is used instead of the signum function sgn$(\cdot)$ to avoid the chattering caused by the discontinuity.

2) IMPACT ANGLE CONTROL COMPOSITE GUIDANCE

IACCG is composed of modified deviated pure pursuit (DPP) for the initial phase and pure proportional navigation (PPN) for the terminal phase. The guidance command is switched from DPP to PPN when a specific condition on the LOS angle is satisfied. The purpose of the initial phase was to guide the missile until it reaches the point from which the missile results in intercepting the target at the desired terminal impact angle when PPN was used. DPP was chosen as the guidance law for the initial phase because it can directly command the look angle inside the FOV limit.

The guidance law is given as

$$a_M = \begin{cases} V_M \dot{\lambda} + K\,(\sigma_c - \sigma_M), & \text{for } |\lambda| < |\lambda_s| \\ N V_M \dot{\lambda}, & \text{for } |\lambda| \geq |\lambda_s| \end{cases} \tag{63}$$

where K is the feedback gain of the look angle error, σ_c denotes the look angle command for DPP, N is the navigation gain for PPN, and λ_s is the LOS angle condition on which switching occurs. The expression for λ_s is given as

$$\lambda_s = \frac{N}{N-1}\left(\tan^{-1}\left(\frac{\sin \gamma_d - \eta \sin \gamma_T}{\cos \gamma_d - \eta \cos \gamma_T}\right) - \frac{\gamma_d - \sigma_c}{N}\right) \tag{64}$$

where γ_d is the desired terminal flight path angle of the missile, γ_T is the flight path angle of the target, and $\eta = V_T/V_M$ is the speed ratio of the target and missile. Note that $\eta = 0$ in this study because the target is assumed to be stationary.

TABLE 1. Simulation parameters.

Category	Parameters	Values
Missile	V_M	200 m/s
	a_{lim}	10 g
	γ_d	-45°
Seeker	$\sigma_{M,\text{sat}}$	7.5°
	$\sigma_{M,\text{lim}}$	10°
IACGBOM	k_2	10
	R_f	0.5
	ϕ_1	0.15
IACCG	N	3
	K	300
EKF/TKF	P_0	$\text{diag}(0.0052, 50)$
	σ_w	0.1
	σ_v	0.0052
	τ_h	7.5°
	τ_l	-7.5°

V. NUMERICAL SIMULATION

In this section, numerical simulation was performed to demonstrate the characteristics and benefits of the TKF-based guidance filter. First, numerical simulation results of an individual engagement scenario are presented for the proposed guidance filter and EKF-based guidance filter. Then, it is demonstrated that the proposed guidance filter can improve the success rate of interception of missiles equipped with a strap-down SAL seeker. Finally, capture regions are compared for the proposed method and EKF-based guidance filter for various parameters of the guidance laws.

A. SIMULATION SETTING

The parameters summarized in this section are commonly used in sections V-B and V-C. The common parameters related to the guidance system are summarized in Table 1. a_{lim} is the acceleration limit of the missile. P_0 is the initial state error covariance matrix. The initial estimate $\hat{x}_0$ of the filter is given by adding the random noise corresponding to P_0 to the initial look angle and relative distance. An algorithm is proposed in [6] for selecting the proper value of K for IACCG when an engagement scenario is given. However, in this study, K is set to be a constant value over all engagement scenarios for simplicity and consistency.

B. PERFORMANCE OF THE GUIDANCE FILTER

This section shows the estimation performance of the TKF-based guidance filter in the saturated region. Numerical simulations were performed at a specific engagement geometry with IACGBOM law. The guidance parameters used in this simulation are summarized in Table 1. The details for the engagement scenario are shown in Table 2. The missile was desired to intercept the stationary target at a terminal impact angle of -45°. The initial look angle is denoted as $\sigma_{M,0}$.

TABLE 2. Engagement scenario.

	r_0	λ_0	$\sigma_{M,0}$
Values	7,000 m	-27°	5°

Fig. 6 shows the history of various variables related to the guidance filters. Figs. 6a and 6c show the look angle estimate and error of the EKF-based guidance filter, respectively. Figs. 6b and 6d show the look angle estimate and error of the TKF-based guidance filter, respectively. In Figs. 6a, 6b, the history for the actual look angle (black line), measurement of the seeker (blue line), and estimated look angle (red line) are shown. As soon as the engagement begins, the actual look angle gets out of the linear region of the seeker, and measurements were saturated at 7.5°. The shaded regions with gray color in each figure represent the saturated region of the seeker. It is shown that the look angle estimation performance of the EKF-based guidance filter rapidly decreases in the saturated region. However, it was shown that the TKF-based guidance filter estimates the look angle relatively accurately even in the saturated region. The TKF was designed with a measurement model that can handle saturated measurements. Thus, the performance degradation due to the modeling error was not significant. Accordingly, the TKF-based guidance filter can perform well in the saturated region of the seeker, in which conventional filters cannot operate.

The effective FOV limit of the SAL seeker, which represents the limit of look angles that the guidance filter can utilize, was widened when a TKF-based guidance filter is used since it operates not only in the linear region of the seeker but also in the saturated region. In other words, the available region of the SAL seeker guaranteeing estimation performance can be expanded when the TKF was combined with the SAL seeker.

C. COMPARISON OF THE SUCCESS RATE OF THE INTERCEPTION

This section shows that the TKF-based guidance filter generally improved the success rate of the interception $p_N(r_0, \lambda_0)$ over the region. To evaluate $p_N(r_0, \lambda_0)$, simulations were performed at each initial condition of interest. The set of initial conditions was determined as follows. First, the continuous space of initial engagement conditions of the missile and target was discretized into grid points. The set of initial relative distances between the missile and target, denoted as L_r, was obtained by equally spacing an interval [1000, 10000] m by 250 m. That is,

$$L_r = \{1000, 1250, 1500, \cdots, 10000\} \tag{65}$$

Likewise, the set of initial LOS angles, denoted as L_λ, was obtained for the two guidance laws. L_λ for IACGBOM was obtained by equal spacing [-70°, -20°] by 1°, and L_λ for IACCG was obtained by equal spacing [-60°, -10°] by 1°.

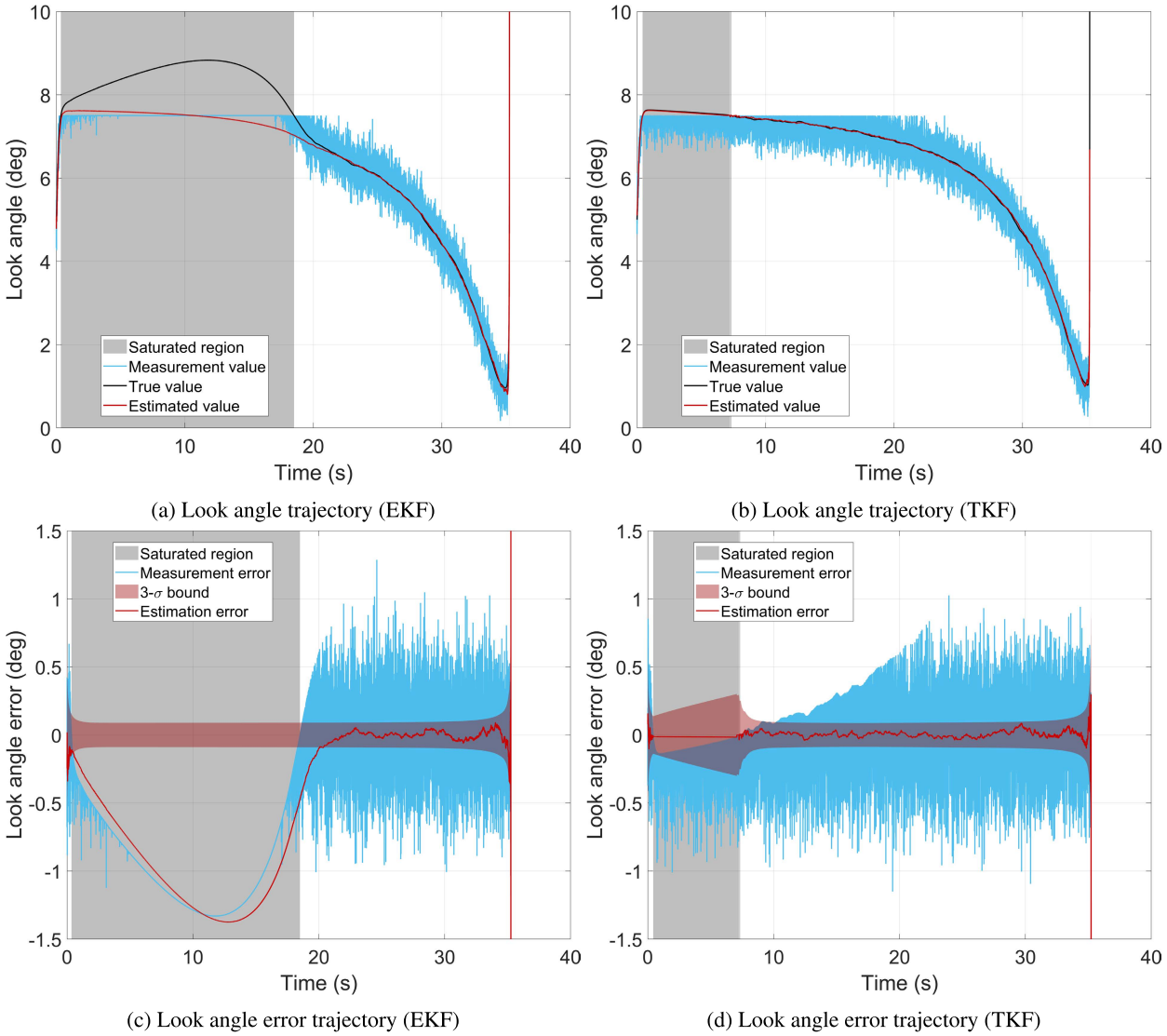

(a) Look angle trajectory (EKF)

(b) Look angle trajectory (TKF)

(c) Look angle error trajectory (EKF)

(d) Look angle error trajectory (TKF)

FIGURE 6. Look angle and look angle error trajectories.

That is,

$$L_\lambda = \begin{cases} \{-70°, -69°, \cdots, -20°\}, & \text{for IACGBOM} \\ \{-60°, -59°, \cdots, -10°\}, & \text{for IACCG} \end{cases} \tag{66}$$

Then, Θ_d is constructed as follows:

$$\Theta_d = \{(r_0, \lambda_0) | r_0 \in L_r, \lambda_0 \in L_\lambda\} \tag{67}$$

For each $(r_0, \lambda_0) \in \Theta_d$, numerical simulations were performed 30 times ($N = 30$) with the same initial conditions except for the different random seeds. The initial look angle $\sigma_{M,0}$ of all simulations is set as zero, which means that a missile is always initially directed toward a target. $p_N(r_0, \lambda_0)$ was calculated according to (32), where the interception of the target is considered to be successful if (29), (30), and (31) are all satisfied. ϵ_r is set to 2 m and ϵ_γ is set to 2.5°.

A comparative simulation is conducted on two cases with different guidance laws. The parameters summarized in Table 1 were used for both cases.

1) CASE1 - IACGBOM

Fig. 7 shows the distribution of $p_N(r_0, \lambda_0)$ when IACGBOM was used as the guidance law. The results were investigated by setting the guidance parameter, k_1, which had a significant effect on the range of look angles, to 7° and 9°, respectively.

In the case when k_1 is set to 7°, it was guaranteed that σ_M remains inside the linear region for all times during the engagement from the formulation of the guidance law. Therefore, the distribution of $p_N(r_0, \lambda_0)$ was almost the same for the EKF and TKF-based guidance systems, as shown in Fig. 7a, 7b.

However, when k_1 is set to 9°, it is allowed for σ_M to exit the linear region. Actually, σ_M exits the linear region

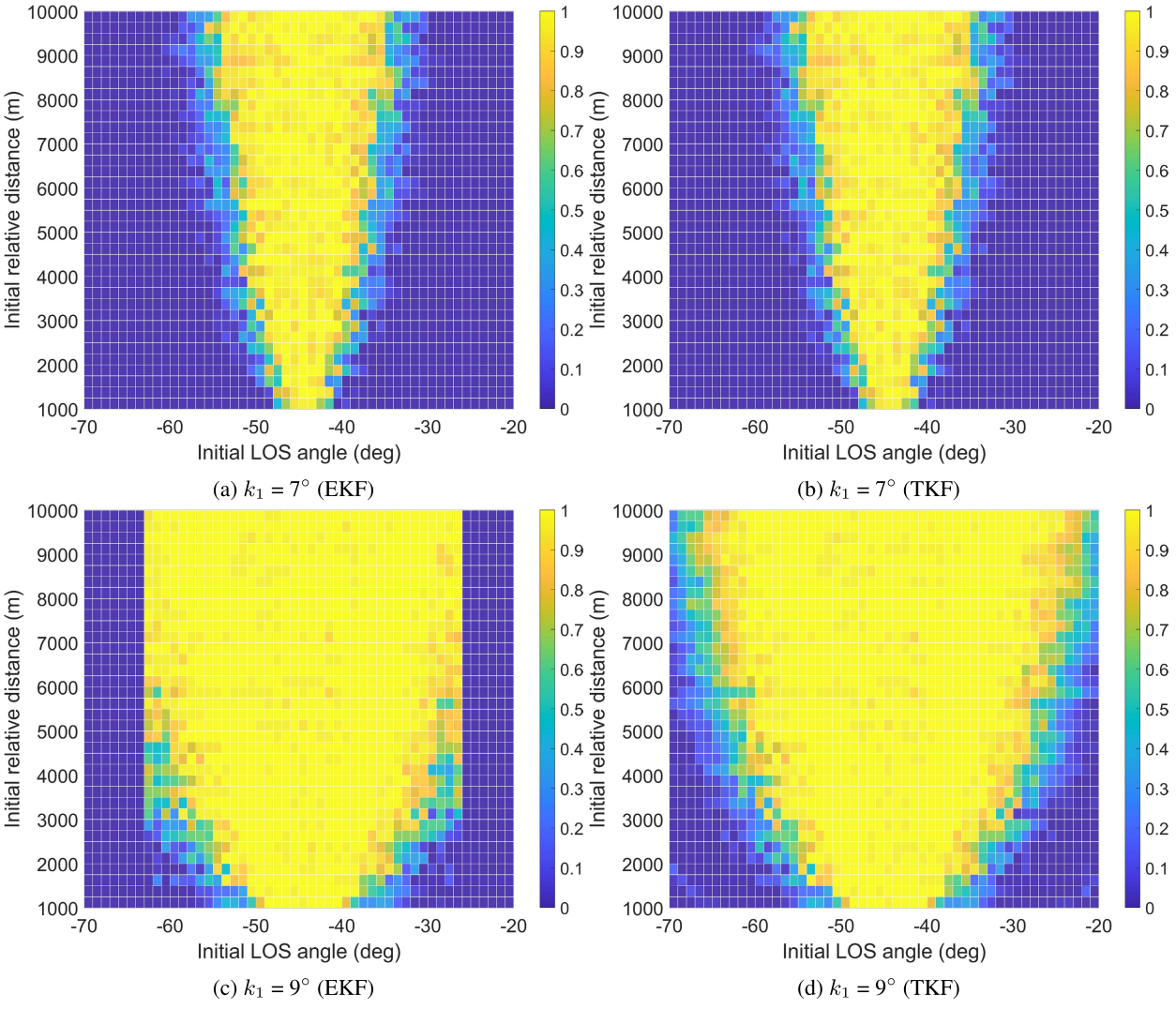

(a) $k_1 = 7^\circ$ (EKF)

(b) $k_1 = 7^\circ$ (TKF)

(c) $k_1 = 9^\circ$ (EKF)

(d) $k_1 = 9^\circ$ (TKF)

FIGURE 7. The distribution of $p_N\ (r_0, \lambda_0)$ for IACGBOM.

for some initial conditions although this was not always the case. For these initial conditions, the TKF-based guidance filter enables the missile to intercept a target while the EKF-based guidance filter cannot. As a result, the region of high $p_N\ (r_0, \lambda_0)$ (yellow region) in Fig. 7d becomes larger than that of Fig. 7c, which means that the TKF-based guidance filter can expand the region of the high success rate of the interception.

2) CASE2 - IACCG

Similarly, in IACCG, one of the guidance parameters σ_c is set to 7° and 8° to compare the results. Fig. 8a and Fig. 8b do not show any notable difference in the distribution of $p_N\ (r_0, \lambda_0)$ of the two guidance filters. According to the IACCG law, the absolute value of the look angle during the entire engagement does not exceed that of σ_c. That is, if the look angle command σ_c is set to 7°, σ_M does not get out of the linear region of the SAL seeker during the engagement. Therefore, the measurements of the seeker do not saturate for all engagements, and the two filters operate identically.

However, if the value of σ_c is set to 8°, the difference in the probability distribution for the EKF and TKF-based guidance systems is significant. Fig. 8c and 8d show that in the case when σ_c is 8°, the capture region of the TKF-based guidance system is much larger than that of the EKF-based guidance system. In this case, σ_M goes beyond the limits of the seeker's linear region. According to the results in Section V-B, the performance of the EKF-based guidance filter may be degraded. As a result, the number of initial conditions for successful interception drastically decreased compared to that of the TKF-based guidance filter. Summarizing the results, the difference in the distribution of $p_N\ (r_0, \lambda_0)$ occurs due to the performance difference between the two filters in the saturated region.

Note from Fig. 8a, 8b, that the region of high $p_N\ (r_0, \lambda_0)$ (yellow region) in each figure is separated into two parts by the strip-shaped region of low $p_N\ (r_0, \lambda_0)$ (dark blue

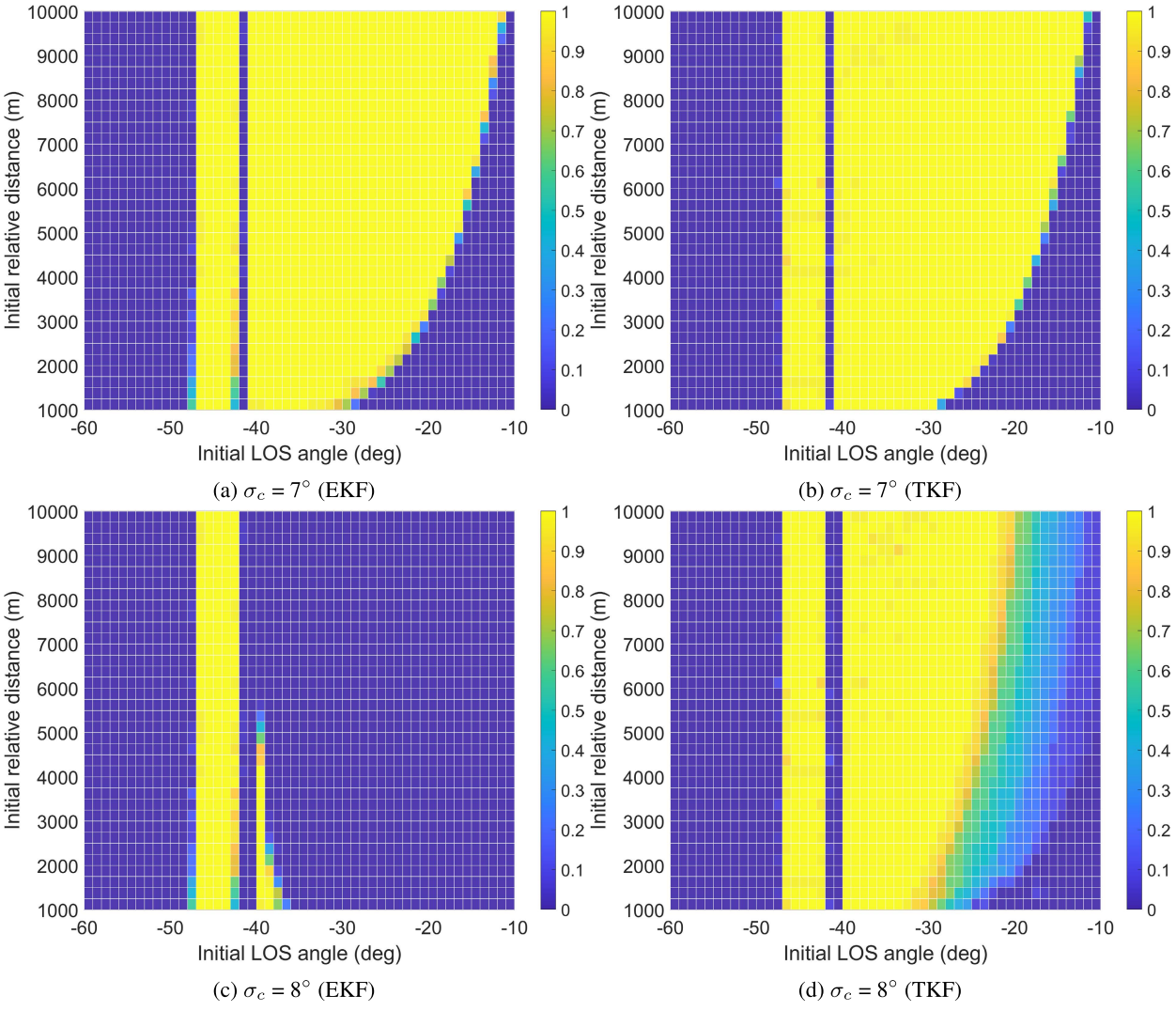

FIGURE 8. The distribution of $p_N(r_0, \lambda_0)$ for IACCG.

strip). The left and right yellow regions originate for different reasons. To explain the reasons, (63) and (64) should be reviewed. The value of λ_s is determined as $\lambda_s = -41.5^\circ$ by using (64) in the setting of Fig. 8a and 8b. The location of the dark blue strip in each figure was near $\lambda_s = -41.5^\circ$, which is not a coincidence. Lookinig onto (63), it was evident that only PPN was used if the LOS angle always satisfies the condition $\lambda \leq \lambda_s$ for $\lambda_s < 0$. The missile follows the line of sight straight from start to end when PPN was used, because $\sigma_0 = 0$ in the simulation setting. Therefore, the missile can intercept the target at γ_d only when the missile starts the engagement at that flight path angle. The initial conditions in the left yellow region correspond to the cases where the missile begins the engagement at the flight path angle close to γ_d and then uses only the PPN. The left yellow region was a strip-shaped region rather than just a line since the success criteria for the interception allow a small terminal impact angle error. The centerline of the left yellow area corresponds to the initial condition $\gamma_{M_0} = \gamma_d$.

D. EXPANSION OF THE CAPTURE REGION

This section finally shows that the proposed guidance filter can increase the size of the capture region over guidance parameters related to the seeker's field of view.

Fig. 9 shows the capture regions for the different values of k_1 of IACGBOM. When the value of k_1 was set to 7°, the capture regions for the two guidance systems were the same. When the value of k_1 was greater than 7°, the capture regions of both guidance systems become larger than for the case when k_1 is 7°. However, when k_1 is 9°, the capture region of the TKF-based guidance system is slightly larger than that of the EKF-based guidance system.

Fig. 10 shows the size of the capture region for different values of σ_c of IACCG. When the value of σ_c is set to 8° or 9°, the capture region was significantly smaller than when σ_c is 7° for both EKF/TKF-based guidance filters. However, when the value of σ_c are 8° or 9°, the size of the capture region of the TKF-based guidance system was much larger than that of the EKF-based guidance system. Therefore, the size of the

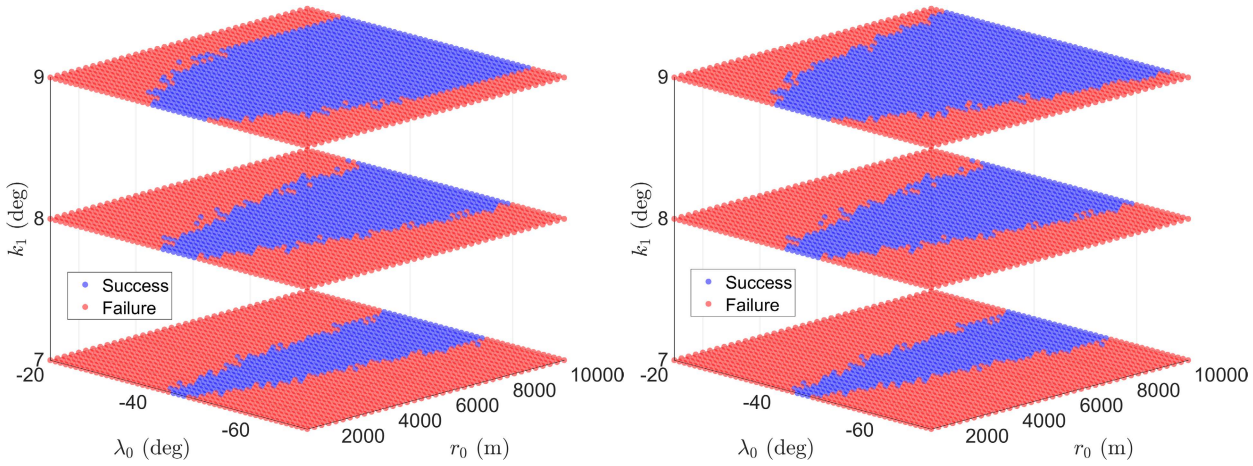

(a) EKF-based guidance filter (b) TKF-based guidance filter

FIGURE 9. Capture region over guidance parameters of IACGBOM.

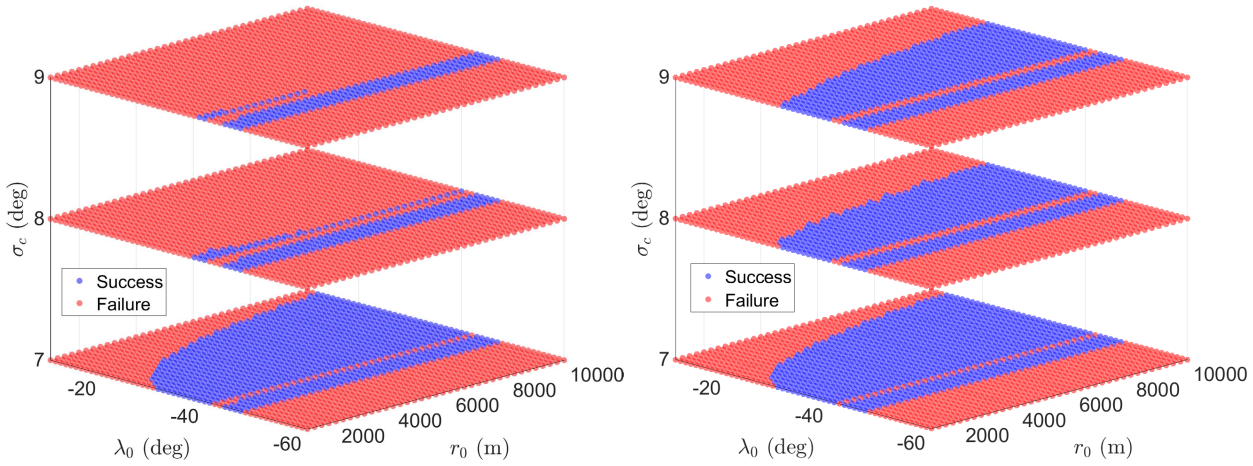

(a) EKF-based guidance filter (b) TKF-based guidance filter

FIGURE 10. Capture region over guidance parameters of IACCG.

TABLE 3. Comparison of the size of the capture region.

Parameter	EKF	TKF	Expansion rate
IACGBOM			
$k_1 = 7.0°$	26.23 %	26.23 %	0.00 %
$k_1 = 8.0°$	41.55 %	41.55 %	0.00 %
$k_1 = 9.0°$	60.83 %	63.33 %	**4.11** %
IACCG			
$\sigma_c = 7.0°$	56.65 %	56.75 %	0.18 %
$\sigma_c = 8.0°$	12.72 %	43.14 %	**239.15** %
$\sigma_c = 9.0°$	10.65 %	42.02 %	**294.55** %

capture region increases when the proposed method was used for both IACCG and IACGBOM.

Table 3 shows the quantitative results of the size of the capture regions. The size of capture region is calculated as

$$\frac{|C_{30}|}{|\Theta_d|} \times 100\ (\%) \tag{68}$$

where $|A|$ for a set A represents the number of elements in the set. In all cases, it can be seen that the size of the capture region of the TKF-based guidance system was larger than or equal to that of the EKF-based one. In summary, it was quantitatively shown that the TKF-based guidance system expanded the size of the capture region.

VI. CONCLUSION

This study proposed the method of designing a guidance filter that can robustly operate in the SAL seeker's saturated region. It was shown that the proposed guidance filter can appropriately cope with saturated measurements and consequently contribute to increasing the size of the capture region. The proposed guidance filter not only works well in normal situations but can also robustly cope with situations in which saturated measurements are given with affordable additional computational loads. However, the performance of the filter

may be degraded if the measurement remains in the saturated region for too long time, as the estimate of the filter may diverge due to the loss of observability. Future work includes analyzing the effect of the residing time in the saturated region on the performance of the filter. Additionally, verifying the performance of the proposed method in more realistic 3-dimensional engagement scenarios will be meaningful.

APPENDIX
FORMULAS FOR TOBIT KALMAN FILTER

In this section, some formulas for the measurement distribution and update stage of the TKF are summarized.

The probability density function of the standard normal distribution is denoted as ϕ.

$$\phi(x) = \frac{1}{\sqrt{2\pi}} \exp\left(-\frac{x^2}{2}\right) \tag{A.1}$$

The cumulative distribution function of the standard normal distribution is denoted as Φ.

$$\Phi(x) = \int_{-\infty}^{x} \phi(\xi) d\xi \tag{A.2}$$

First, the measurement model in (2) and (3) is repeated here for a *scalar* measurement case.

$$z_k^* = Hx_k + v_k \tag{A.3}$$

$$z_k = \begin{cases} z_k^*, & \tau_l < z_k^* < \tau_h \\ \tau_l, & z_k^* \le \tau_l \\ \tau_h, & z_k^* \ge \tau_h \end{cases} \tag{A.4}$$

where $x_k \in \mathbb{R}^{n\times 1}$, $z_k^* \in \mathbb{R}$, $H \in \mathbb{R}^{1\times n}$, and $z_k, \tau_l, \tau_h \in \mathbb{R}$. Also, $v_k \sim N\left(0, \sigma^2\right)$ where N refers to the normal distribution and σ is the standard deviation of the distribution.

According to the law of total expectation, the expectation of the measurement z_k given x_k can be written as

$$\begin{aligned} E\left[z_k|x_k\right] = {} & E\left[z_k|\tau_l < z_k < \tau_h\right] P\left\{\tau_l < z_k < \tau_h\right\} \\ & + E\left[z_k|z_k \le \tau_l\right] P\left\{z_k \le \tau_l\right\} \\ & + E\left[z_k|z_k \ge \tau_h\right] P\left\{z_k \ge \tau_h\right\} \end{aligned} \tag{A.5}$$

where the explicit expression for the dependence of variables on x_k is dropped from right-hand side terms for notational simplicity. The same omission will be used without mentioning if there is no confusion from the context. The probability of z_k being unsaturated is given as

$$\begin{aligned} p_{us} &= P\left\{\tau_l < z_k < \tau_h\right\} \\ &= \Phi\left(\frac{\tau_h - Hx_k}{\sigma}\right) - \Phi\left(\frac{\tau_l - Hx_k}{\sigma}\right) \end{aligned} \tag{A.6}$$

The probabilities of z_k being saturated from above and below are given as

$$p_h = P\left\{z_k \ge \tau_h\right\} = \Phi\left(\frac{Hx_k - \tau_h}{\sigma}\right) \tag{A.7}$$

$$p_l = P\left\{z_k \le \tau_l\right\} = \Phi\left(\frac{\tau_l - Hx_k}{\sigma}\right) \tag{A.8}$$

The expectation of z_k when not saturated is

$$E\left[z_k|\tau_l < z_k < \tau_h\right] = Hx_k - \sigma\lambda\left(\tau_h, \tau_l\right) \tag{A.9}$$

where

$$\lambda\left(\tau_h, \tau_l\right) = \frac{\phi\left(\frac{\tau_h - Hx_k}{\sigma}\right) - \phi\left(\frac{\tau_l - Hx_k}{\sigma}\right)}{p_{us}} \tag{A.10}$$

Also,

$$E\left[z_k|z_k \le \tau_l\right] = \tau_l, \quad E\left[z_k|z_k \ge \tau_h\right] = \tau_h \tag{A.11}$$

Substituting (A.9)-(A.11) into (A.5),

$$E\left[z_k|x_k\right] = p_{us}\left(Hx_k - \sigma\lambda\left(\tau_h, \tau_l\right)\right) + p_l\tau_l + p_h\tau_h \tag{A.12}$$

The variance of z_k given x_k can be written as

$$\begin{aligned} \mathrm{Var}\left(z_k|\tau_l < z_k < \tau_h\right) = {} & E\left[z_k^2|\tau_l < z_k < \tau_h\right] \\ & - \left(E\left[z_k|\tau_l < z_k < \tau_h\right]\right)^2 \end{aligned} \tag{A.13}$$

Here,

$$\begin{aligned} E\left[z_k^2|\tau_l < z_k < \tau_h\right] = {} & (Hx_k)^2 + \sigma^2 - \sigma Hx_k\lambda\left(\tau_h, \tau_l\right) \\ & + \sigma\frac{\tau_l\phi\left(\frac{\tau_l - Hx_k}{\sigma}\right) - \tau_h\phi\left(\frac{\tau_h - Hx_k}{\sigma}\right)}{p_{us}} \end{aligned} \tag{A.14}$$

Substituting (A.9) and (A.14) into (A.13),

$$\begin{aligned} & \mathrm{Var}\left(z_k|\tau_l < z_k < \tau_h\right) \\ & = \sigma^2\left(1 - \lambda^2\left(\tau_h, \tau_l\right)\right) \\ & \quad + \sigma Hx_k\lambda\left(\tau_h, \tau_l\right) + \sigma\frac{\tau_l\phi\left(\frac{\tau_l - Hx_k}{\sigma}\right) - \tau_h\phi\left(\frac{\tau_h - Hx_k}{\sigma}\right)}{p_{us}} \end{aligned} \tag{A.15}$$

Note that $z_k = Hx_k + v_k$. Therefore,

$$\mathrm{Var}\left(z_k|\tau_l < z_k < \tau_h\right) = \mathrm{Var}\left(v_k|\tau_l < z_k < \tau_h\right) \tag{A.16}$$

Now, consider the general m-dimensional *vector* measurement case with $z_k^* \in \mathbb{R}^{m\times 1}$, $H \in \mathbb{R}^{m\times n}$, and $z_k, \tau_l, \tau_h \in \mathbb{R}^{m\times 1}$. Also, assume that $v_k \sim N(0, R)$ where

$$R = \mathrm{diag}\left(\sigma(1)^2, \sigma(2)^2, \cdots, \sigma(m)^2\right) \tag{A.17}$$

Then, the variance of the i th element of v_k

$$\mathrm{Var}\left(v_k(i)|\tau_l(i) < z_k(i) < \tau_h(i)\right) \tag{A.18}$$

can be evaluated by replacing every scalar variable in (A.15) with the i th element of the corresponding vector variable. That is, (A.15) is evaluated elementwise for the vector measurement case.

REFERENCES

[1] J. I. Lee, I.-S. Jeon, and M.-J. Tahk, "Guidance law to control impact time and angle," *IEEE Trans. Aerosp. Electron. Syst.*, vol. 43, no. 1, pp. 301–310, Jan. 2007, doi: 10.1109/TAES.2007.357135.

[2] Y. I. Lee, S. H. Kim, and M.-J. Tahk, "Optimality of linear time-varying guidance for impact angle control," *IEEE Trans. Aerosp. Electron. Syst.*, vol. 48, no. 4, pp. 2802–2817, Oct. 2012, doi: 10.1109/TAES.2012.6324662.

[3] C.-H. Lee, M.-J. Tahk, and J.-I. Lee, "Generalized formulation of weighted optimal guidance laws with impact angle constraint," *IEEE Trans. Aerosp. Electron. Syst.*, vol. 49, no. 2, pp. 1317–1322, Apr. 2013, doi: 10.1109/TAES.2013.6494416.

[4] B.-G. Park, T.-H. Kim, and M.-J. Tahk, "Range-to-go weighted optimal guidance with impact angle constraint and seeker's look angle limits," *IEEE Trans. Aerosp. Electron. Syst.*, vol. 52, no. 3, pp. 1241–1256, Jun. 2016, doi: 10.1109/TAES.2016.150415.

[5] C.-H. Lee and M.-G. Seo, "New insights into guidance laws with terminal angle constraints," *J. Guid., Control Dyn.*, vol. 41, no. 8, pp. 1832–1837, Aug. 2018, doi: 10.2514/1.G002817.

[6] B.-G. Park, H.-H. Kwon, Y.-H. Kim, and T.-H. Kim, "Composite guidance scheme for impact angle control against a nonmaneuvering moving target," *J. Guid., Control, Dyn.*, vol. 39, no. 5, pp. 1132–1139, May 2016, doi: 10.2514/1.G001547.

[7] B. S. Kim, J. G. Lee, and H. S. Han, "Biased PNG law for impact with angular constraint," *IEEE Trans. Aerosp. Electron. Syst.*, vol. 34, no. 1, pp. 277–288, Jan. 1998, doi: 10.1109/7.640285.

[8] B.-G. Park, T.-H. Kim, and M.-J. Tahk, "Biased PNG with terminal-angle constraint for intercepting nonmaneuvering targets under physical constraints," *IEEE Trans. Aerosp. Electron. Syst.*, vol. 53, no. 3, pp. 1562–1572, Jun. 2017, doi: 10.1109/TAES.2017.2667518.

[9] S. Kumar, S. Rao, and D. Ghose, "Sliding-mode guidance and control for all-aspect interceptors with terminal angle constraints," *J. Guid., Control Dyn.*, vol. 35, no. 4, p. 1111, 2012, doi: 10.2514/1.55242.

[10] D. Cho, H. J. Kim, and M.-J. Tahk, "Impact angle constrained sliding mode guidance against maneuvering target with unknown acceleration," *IEEE Trans. Aerosp. Electron. Syst.*, vol. 51, no. 2, pp. 1310–1323, Apr. 2015, doi: 10.1109/TAES.2015.140358.

[11] K. S. Erer, R. Tekin, and M. K. Ozgoren, "Look angle constrained impact angle control based on proportional navigation," in *Proc. AIAA Guid., Navigat., Control Conf.*, Jan. 2015, p. 91.

[12] S. He, D. Lin, and J. Wang, "Integral global sliding mode guidance for impact angle control," *IEEE Trans. Aerosp. Electron. Syst.*, vol. 55, no. 4, pp. 1843–1849, Aug. 2019, doi: 10.1109/TAES.2018.2876588.

[13] J. Yun, C.-K. Ryoo, and T.-L. Song, "Strapdown sensors and seeker based guidance filter design," in *Proc. Int. Conf. Control, Autom. Syst.*, Oct. 2008, pp. 468–472, doi: 10.1109/ICCAS.2008.4694686.

[14] Y. Wang, J. Wang, S. He, H.-S. Shin, and A. Tsourdos, "Optimal guidance with active observability enhancement for scale factor error estimation of strapdown seeker," *IEEE Trans. Aerosp. Electron. Syst.*, vol. 57, no. 6, pp. 4347–4362, Dec. 2021, doi: 10.1109/TAES.2021.3096870.

[15] S. Zhou, S. Zhang, and D. Wang, "Impact angle control guidance law with seeker's field-of-view constraint based on logarithm barrier Lyapunov function," *IEEE Access*, vol. 8, pp. 68268–68279, 2020, doi: 10.1109/ACCESS.2020.2986355.

[16] A. Dhar and D. Ghose, "Capture region for a realistic TPN guidance law," *IEEE Trans. Aerosp. Electron. Syst.*, vol. 29, no. 3, pp. 995–1003, Jul. 1993, doi: 10.1109/7.220946.

[17] F. Tyan, "The capture region of a general 3D TPN guidance law for missile and target with limited maneuverability," in *Proc. Amer. Control Conf.*, Jun. 2001, pp. 512–517, doi: 10.1109/ACC.2001.945597.

[18] F. Tyan, "Capture region of a GIPN guidance law for missile and target with bounded maneuverability," *IEEE Trans. Aerosp. Electron. Syst.*, vol. 47, no. 1, pp. 201–213, Jan. 2011, doi: 10.1109/TAES.2011.5705670.

[19] L.-J. Liu and Y. Shen, "Three-dimension H_∞ guidance law and capture region analysis," *IEEE Trans. Aerosp. Electron. Syst.*, vol. 48, no. 1, pp. 419–429, Jan. 2012, doi: 10.1109/TAES.2012.6129645.

[20] X. Xu and C. Guo, "Capture zone of biased proportional navigation guidance law," in *Proc. IEEE Int. Conf. Inf. Autom.*, Aug. 2015, pp. 927–930, doi: 10.1109/ICInfA.2015.7279419.

[21] Z. Jin, S. Lei, W. Huaji, Z. Dayuan, and L. Humin, "Optimal mid-course trajectory planning considering the capture region," *J. Syst. Eng. Electron.*, vol. 29, no. 3, pp. 587–600, 2018, doi: 10.21629/JSEE.2018.03.16.

[22] A. Filgoz, G. Demirezen, and M. U. Demirezen, "Applying novel adaptive activation function theory for launch acceptability region estimation with neural networks in constrained hardware environments: Performance comparison," in *Proc. IEEE/AIAA 40th Digit. Avionics Syst. Conf. (DASC)*, Oct. 2021, pp. 1–10, doi: 10.1109/DASC52595.2021.9594334.

[23] K. S. Yoon, J. H. Park, I. G. Kim, and K. S. Ryu, "New modeling algorithm for improving accuracy of weapon launch acceptability region," in *Proc. 29th Digit. Avionics Syst. Conf.*, Oct. 2010, p. 6, doi: 10.1109/DASC.2010.5655454.

[24] J. J. Seo, "Developing an algorithm to calculate launch acceptability region of air-to-ground guided bomb," *J. Korean Soc. Aeronaut. Space Sci.*, vol. 45, no. 6, pp. 517–522, Jun. 2017.

[25] S. Kim, J. Park, S. Park, S. Lee, and K. Kim, "Computation for launch acceptability region of air-to-surface guided bomb using artificial neural network," *J. Korean Soc. Aeronaut. Space Sci.*, vol. 46, no. 4, pp. 283–289, Apr. 2018.

[26] D. R. L. Güner, "Modeling of a generic laser guided weapon with velocity pursuit guidance and its performance analysis using various control strategies," M.S. thesis, Dept. Mech. Eng., Middle East Tech. Univ., Ankara, Turkey, 2004.

[27] Z. Ying-chun, L. Jing-jing, and L. Hua-yi, "Line of sight rate estimation of strapdown imaging seeker based on particle filter," in *Proc. 3rd Int. Symp. Syst. Control Aeronaut. Astronaut.*, Jun. 2010, pp. 191–195, doi: 10.1109/ISSCAA.2010.5633193.

[28] J. M. Maley, "Line of sight rate estimation for guided projectiles with strapdown seekers," in *Proc. AIAA Guid., Navigat., Control Conf.*, Jan. 2015, p. 344, doi: 10.2514/6.2015-0344.

[29] C. Wei, Y. Han, N. Cui, and H. Xu, "Fifth-degree cubature Kalman filter estimation of seeker line-of-sight rate using augmented-dimensional model," *J. Guid., Control, Dyn.*, vol. 40, no. 9, pp. 2355–2362, Sep. 2017, doi: 10.2514/1.G002809.

[30] Z. Di, H. Zhiheng, and Z. Wenxue, "Accurate estimation of line-of-sight rate under strong impact interference effect," *J. Syst. Eng. Electron.*, vol. 31, no. 6, pp. 1262–1273, Dec. 2020, doi: 10.23919/JSEE.2020.000097.

[31] B. Allik, "The tobit Kalman filter: An estimator for censored data," Ph.D. dissertation, Dept. Elect. Comput. Eng., Univ. Delaware, Newark, Delaware, 2014.

[32] B. Allik, C. Miller, M. J. Piovoso, and R. Zurakowski, "The tobit Kalman filter: An estimator for censored measurements," *IEEE Trans. Control Syst. Technol.*, vol. 24, no. 1, pp. 365–371, Jan. 2016, doi: 10.1109/TCST.2015.2432155.

[33] H. Geng, Z. Wang, Y. Liang, Y. Cheng, and F. E. Alsaadi, "Tobit Kalman filter with fading measurements," *Signal Process.*, vol. 140, pp. 60–68, Nov. 2017.

[34] H. Geng, Z. Wang, Y. Liang, Y. Cheng, and F. E. Alsaadi, "Tobit Kalman filter with time-correlated multiplicative sensor noises under redundant channel transmission," *IEEE Sensors J.*, vol. 17, no. 24, pp. 8367–8377, Dec. 2017, doi: 10.1109/JSEN.2017.2766077.

[35] E. A. Wan and R. Van Der Merwe, "The unscented Kalman filter for nonlinear estimation," in *Proc. IEEE Adapt. Syst. Signal Process., Commun., Control Symp.*, Oct. 2000, pp. 153–158, doi: 10.1109/ASSPCC.2000.882463.

[36] H.-G. Kim, J.-Y. Lee, and H.-J. Kim, "Look angle constrained impact angle control guidance law for homing missiles with bearings-only measurements," *IEEE Trans. Aerosp. Electron. Syst.*, vol. 54, no. 6, pp. 3096–3107, Dec. 2018, doi: 10.1109/TAES.2018.2843600.

[37] J.-H. Hong, S.-S. Park, C.-H. Lee, and C.-K. Ryoo, "Study on parasite effect with strapdown seeker in consideration of time delay," *J. Guid., Control, Dyn.*, vol. 42, no. 6, pp. 1383–1392, Jun. 2019, doi: 10.2514/1.G004040.

[38] P. Zarchan and H. Musoff, "Polynomial Kalman filters," in *Fundamentals Kalman Filtering: A Practical Approach*, 2nd ed. Reston, VA, USA: AIAA, 2015, Ch. 4, Sec. 1, pp. 165–186.

YOUNGJUN LEE received the B.S. degree in mechanical aerospace engineering from Seoul National University, Republic of Korea, in 2019, where he is currently pursuing the Ph.D. degree in aerospace engineering. His current research interests include data-driven missile control, optimization, and guidance system of missiles.

SANGMIN LEE received the B.S. degree in mechanical and aerospace engineering from Seoul National University, Republic of Korea, in 2019, where he is currently pursuing the Ph.D. degree in aerospace engineering. He is mainly interested in the application of unmanned aerial vehicles for various purposes. His current research interests include application of data-driven methods to path-planning, guidance, and control.

YOUDAN KIM (Senior Member, IEEE) received the B.S. and M.S. degrees in aeronautical engineering from Seoul National University, Republic of Korea, in 1983 and 1985, respectively, and the Ph.D. degree in aerospace engineering from Texas A&M University, in 1990. In 1992, he joined Seoul National University as a Faculty Member, where he is currently a Professor with the Department of Aerospace Engineering. His current research interests include aircraft control system design, reconfigurable control system design, path planning, and guidance techniques for aerospace systems.

YONGSU HAN received the B.S. degree in mechanical and aerospace engineering from Sejong University, Republic of Korea, in 2004, and the M.S. and Ph.D. degrees in aerospace engineering from Seoul National University, Republic of Korea, in 2006 and 2012, respectively. He is currently working as a Research Fellow with LIG Nex1 Company Ltd., South Korea. His research interests include performance analysis and guidance for guided munitions.

JANGSEONG PARK received the B.S. degree in aerospace engineering from the University of Inha, Incheon, South Korea, in 2011, and the M.S. degree in aerospace engineering from KAIST, Daejeon, South Korea, in 2013, respectively. In 2013, he joined LIG Nex1 Company Ltd., for development of precision guided missiles. His research interests include guidance and filter design.

GYEONG-HUN KIM received the B.S. and M.S. degrees in aerospace engineering from Chungnam National University, Daejeon, South Korea, in 2014 and 2016, respectively. He is currently with LIG Nex1 Company Ltd., South Korea. His research interests include guidance and control for guided munitions.